Nano Today 56 (2024) 102247

Contents lists available at ScienceDirect

Nano Today

journal homepage: www.elsevier.com/locate/nanotoday

Ultra-confined controllable cyclic peptides as supramolecular biomaterials

Mey-Sam Chorsi [a,b,c,d,e,*], Will Linthicum [f], Alexandra Pozhidaeva [g], Caitlyn Mundrane [b], Vikram Khipple Mulligan [h], Yihang Chen [i], Pouya Tavousi [a], Vitaliy Gorbatyuk [j], Olga Vinogradova [k], Jeffrey C. Hoch [g], Bryan D. Huey [f], Thanh D. Nguyen [a,b,l,m], H. Tom Soh [c,d,e], Kazem Kazerounian [a,b], Horea Ilies [a,b,**]

[a] School of Mechanical, Aerospace, and Manufacturing Engineering, University of Connecticut, 06030-3305, Storrs, CT 06269, USA
[b] Department of Biomedical Engineering, University of Connecticut, Storrs, CT 06269, USA
[c] Department of Bioengineering, Stanford University, Stanford, CA 94305, USA
[d] Department of Radiology, Stanford University, Stanford, CA 94305, USA
[e] Department of Electrical Engineering, Stanford University, Stanford, CA 94305, USA
[f] Department of Materials Science and Engineering, University of Connecticut, Storrs, CT 06269, USA
[g] Department of Molecular Biology and Biophysics, UConn Health, Farmington, CT 06030, USA
[h] Center for Computational Biology, Flatiron Institute, New York, NY 10010, USA
[i] Department of Materials Science and Engineering, Stanford University, Stanford, CA 94305, USA
[j] Department of Chemistry, University of Connecticut, Storrs, CT 06269, USA
[k] Department of Pharmaceutical Sciences, University of Connecticut, Storrs, CT 06269, USA
[l] Polymer Program, University of Connecticut, Storrs, CT 06269, USA
[m] Institute of Materials Science, University of Connecticut, Storrs, CT 06269, USA

ARTICLE INFO

Keywords:
Peptides
Cyclic amino acids
Supramolecular biomaterials
Self-assembly

ABSTRACT

The capacity to design molecules capable of orchestrated movements in response to specific stimuli could yield functional biomaterials suitable for diverse innovative materials and devices. However, the rational design of molecules capable of precisely orchestrated movements remains exceedingly difficult. As a stepping-stone toward this goal, we have developed a method for manufacturing precisely designed cyclic peptide molecules with a single degree of freedom. We demonstrate that the structural configuration of these molecules can be precisely determined under different external stimuli and explore the mechanism by which these molecules form supramolecular self-assemblies. Our experimental analysis of these assemblies reveals that our constrained cyclic peptides form nanotube structures through sheet-like hydrogen bonding. Unexpectedly, these higher-order structures can achieve remarkably rigid (~10 GPa) and stable architectures at high temperatures—comparable to the most rigid proteinaceous materials in nature. The design strategy described here could facilitate the development of molecular machines, smart materials, and other applications that require fine-tuned regulation of biomolecular behavior.

Introduction

Controllable biomolecules move in a well-defined way in response to external stimuli. Through careful design and engineering, the properties, functions, and interactions of these molecules can be modulated, allowing for targeted applications in fields such as drug delivery [1–5], biomaterials [6,7], biosensing [8], and bioimaging [9]. These biomolecules can be triggered by various stimuli such as light [10–19], temperature [20–22], chemical reactions [23–27], electrical potential [28–31], or mechanical stress [32–36]. They may be assembled from a diverse range of biomolecular components, including nucleic acids [37–42], carbohydrates [43–46], lipids [47–50], proteins [51–57], and peptides [58–64]. Peptides are particularly well-suited for this purpose due to their structural diversity, specificity, functional versatility, biocompatibility, and synthetic accessibility [65–67].

Controllable biomolecules could offer numerous opportunities for

* Correspondence to: Stanford University, Stanford, CA 94305, USA.
** Correspondence to: University of Connecticut, Storrs, CT 06269, USA.
E-mail addresses: chorsi@stanford.edu (M.-S. Chorsi), horea.ilies@uconn.edu (H. Ilies).

https://doi.org/10.1016/j.nantod.2024.102247
Received 8 September 2023; Received in revised form 25 February 2024; Accepted 24 March 2024
Available online 1 April 2024

precise functionalization of supramolecular biomaterials. Supramolecular materials are composed of molecular building blocks that can self-assemble through non-covalent interactions to form hierarchical structures [68,69]. By incorporating controllable biomolecules, it becomes possible to precisely manipulate the properties and behavior of supramolecular biomaterials at the molecular level. This control allows for the design and creation of biomaterials with enhanced functionality, improved stability, and tailored interactions with their surrounding environment [70–76]. Controllability can enable precise regulation of the assembly and disassembly processes within supramolecular biomaterials [77–81]. This control over molecular organization empowers the development of biomaterials with specific structural arrangements, such as hierarchical architectures or dynamic systems [82–84]. These structures can exhibit unique mechanical [85,86], chemical [87,88], or optical properties [89–91], leading to applications in tissue engineering [92,93], drug delivery [94–96], regenerative medicine [97,98], and biosensing.

Peptide-based supramolecular biomaterials also offer other distinctive advantages [99–105]. They can have structural features at different length scales, ranging from nanoscale to macroscale, and their properties can be tuned by modifying the amino acid sequence, length, or other design parameters [106–115]. One notable example of such materials is peptide-based glass, which exhibits promising biocompatibility and biodegradability profiles, making it an attractive candidate for use in various biomedical contexts [116].

However, it should be noted that controlling the precise arrangement and movement of biomolecules remains challenging, and this complexity can be further amplified by the demands of physiological conditions and the potential need for intricate chemical synthesis processes. For example, the rapid degradation of peptides in biological environments limits the long-term durability of peptide biomaterials. To counter this issue, cyclic peptides can be employed that mitigate degradation by eliminating the C and N termini of peptides [117,118]. Cyclic peptides also offer other advantages over linear peptides, including improved binding affinity, increased membrane permeability, and diverse target engagement [119–122]. These characteristics make cyclic peptides promising candidates for supramolecular biomaterials design [123–126]. Unfortunately, there is currently no general strategy to effectively combine existing cyclic peptides and construct larger functional biomaterials from smaller constituent parts. Furthermore, the *de novo* design of cyclic peptides—offering atomic-scale control over both structure and molecular motion—remains challenging.

Over the past 20 years, our group has developed a novel approach for designing biomolecules with controllable motion and function based on kinematic principles [127–133]. Our working hypothesis has been that the creation of controllable molecules will first require the *de novo* design of molecules with well-defined structures and well-confined motions, and that this can be achieved by rationally designing molecules with only a single effective degree of freedom (DOF) of motion. Here, we expand on our prior work by designing and synthesizing the simplest cyclic peptides that can be precisely controlled. Although these molecules possess many rotatable bonds, they are engineered to have a single effective DOF; for this reason, we refer to them as 1-DOF linkages. Our hierarchical design process allows for the development of diverse classes of biomolecules with different numbers of amino acids and amino acid types. We explore experimental and theoretical means of altering the structure of these cyclic peptides by introducing external stimuli such as heat and external electric fields to control their motion. Furthermore, we demonstrate experimentally that these controllable biomolecules self-assemble into higher-order structures and present a model for self-assembly based on these results. These supramolecular assemblies exhibit remarkably rigid and stable architectures at high temperatures. We propose that such structural architectures could be used to produce larger multifunctional materials based on the collective motion of molecular subunits, which could in turn be applied towards the development of new biocompatible and biodegradable materials.

Results

Design, synthesis, and structural characterization of single controllable cyclic peptides

By pursuing a structure limited to 1-DOF, we greatly confine the mobility of the molecules so that their behavior can be described with just a single parameter, which ensures that the system behaves in a reproducible and predictable way. Based on these design principles, almost every amino acid can be modeled as a 2-DOF linkage corresponding to the ϕ and ψ dihedral angles, and these dihedral angles enable us to determine the overall structure of the linkage. Proline is an exception to this rule with only one freely-rotatable dihedral angle, ψ. As described below, we can generate 1-DOF mechanisms by creating combinations of amino acids with carefully chosen numbers of prolines.

To begin, we chose a simple spatial 1-DOF design: a closed-loop seven-bar linkage (*i.e.*, the closed-loop form of a 7-DOF linear peptide) [134]. The requirement that the rigid-body transform from the end of the loop to the start in this construct must be compatible with an amide bond fixes six DOFs, leaving only one “free” DOF. This linkage can be designed from a linear peptide chain with seven body vectors (links, L) and seven rotatable dihedral angles (joints, J), as shown in Figs. S1-S5. As proline is the only amino acid with L=1 and J=1, the presence of one proline in a four-residue cyclic peptide (class I), three prolines in a five-residue peptide (class II or III), five prolines in a six-residue peptide (class IV), or seven prolines in a seven-residue peptide (class V) all result in a seven-bar linkage. For non-proline residues, glycine is prefered due to the lack of side chain; however, we used cysteine in some cases where the chemical synthesis of the molecule was not possible. For each of these macrocycle constructs, there is a single unique sequence of proline and non-proline residues with the desired proline count—with the exception of the five-residue cyclic peptide, in which two patterns of three prolines and two non-prolines are possible (Fig. 1**a**; class II and class III). Loop closure creates a cyclic structure, biologically analagous to a cyclic peptide, and fixes six DOF, effectively reducing a 7-DOF linear peptide to a 1-DOF cyclic peptide (Fig. 1**b**). We have detailed our kinetostatic design strategy in **Supplementary Note S1**.

We synthesized the designed cyclic biomolecules using standard head-to-tail cyclic Fmoc solid-phase peptide synthesis (see **Methods**, Figs. S6-S11, and **Supplementary Note S2**). We experimentally determined the structures of the peptides using nuclear magnetic resonance spectroscopy (NMR; see **Methods** and Figs. S12-S14). Up to 20 NMR structure candidates with the lowest energies for class I, class II, and class III were then compared with their design model (Fig. 1**b**). NMR structures could not be obtaind for class IV and class V cyclic peptides due to the high degree of magnetic equivalence among nuclei, and so we have instead compared our design model with structures predicted by the Rosetta software (see **Methods**, **Supplementary Note S3**). Rosetta has been used previously to validate designed peptides, and several examples of accurate prediction of peptide structure by Rosetta have been published [135–139]. We calculated relatively low root mean square deviations (RMSD) from the designed model (within 1 Å) for the class I–III NMR structures, suggesting that our peptides are structured as designed. Rosetta predictions also correlated closely with the NMR structures in these cases based on RMSD values, suggesting that such predictions offer a good point of comparison in other cases in which NMR structures could not be obtained (energy landscapes are shown in Fig. S15). The class IV peptide showed close agreement between Rosetta prediction and design model, with a backbone RMSD of 1.26 Å. The class V peptide showed a somewhat more heterogeneous low-energy population in the Rosetta simulation, suggesting less rigid folding, although the backbone RMSD still remained fairly low at 1.62 Å. This suggests that the kinematic method used for design, which assumes ideal bond lengths and bond angles, perfectly planar peptide bonds, and optimal proline ϕ dihedrals, produces structures that remain reasonably well-folded even in Rosetta simulations in which all of these values are

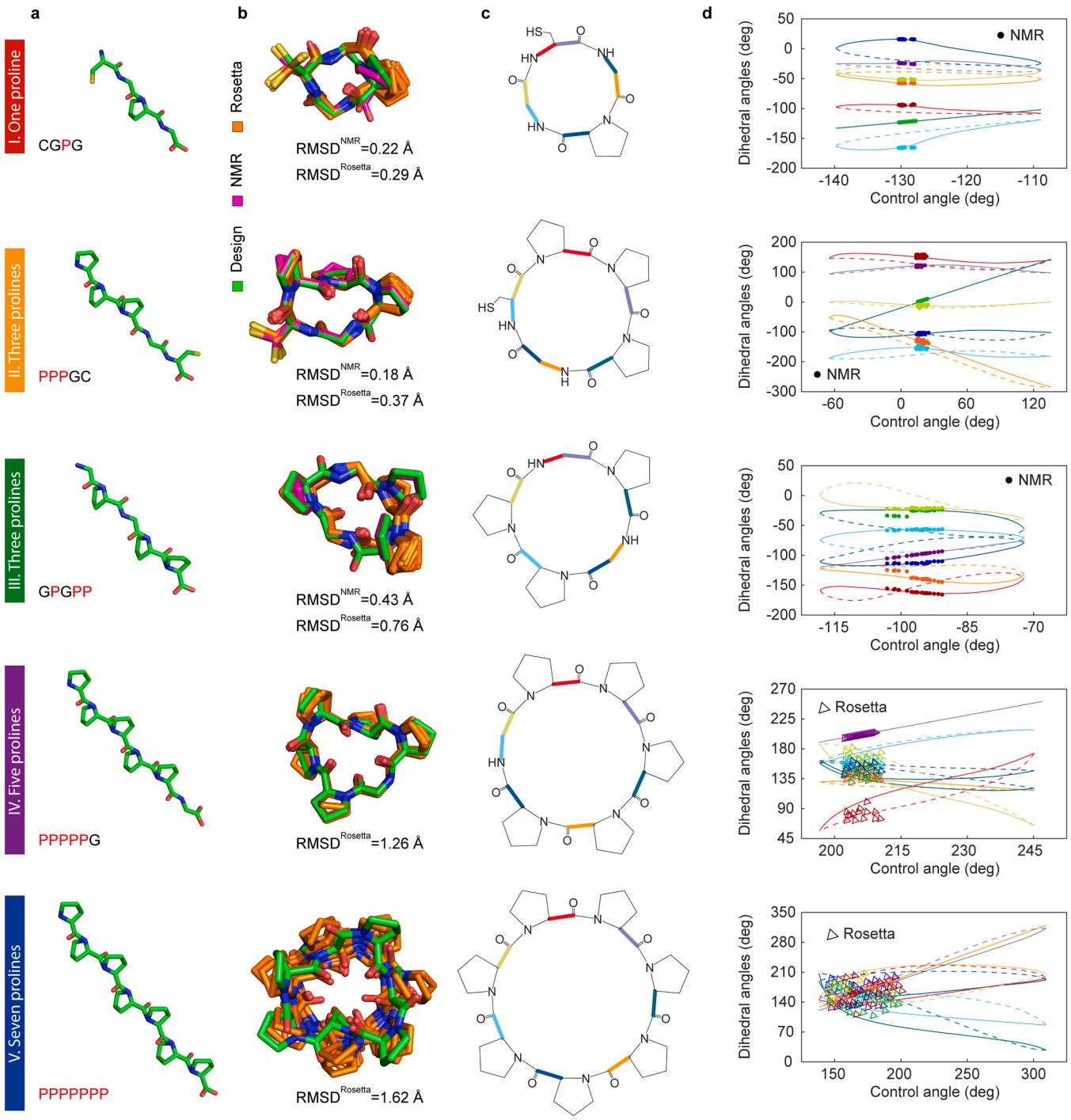

Fig. 1. Design, synthesis, and structural characterization of single controllable cyclic peptides. **a**, Open chain structure of five classes of controllable cyclic peptide comprising proline and non-proline (glycine or cysteine) residues with exactly seven rotatable bonds in the backbone. Prolines are highlighted in red in the sequences, which were also synthesized for experimental characterization. **b**, Closed-chain structure of the peptides presented in **a**. We compared the configuration of the designed peptides (green) to NMR (magenta) and Rosetta predictions (orange). We report the backbone heavy atom RMSDs of the designed structure relative to the closest member of the NMR ensemble (for class I–III) or the lowest-energy Rosetta prediction (for all classes). RMSD values are low in all cases, although we predict some conformational heterogeneity is predicted for the 7-residue (class V) cyclic peptide. **c**, 2D structure of the peptides in **b**. The rotatable backbone dihedral angles of each amino acid are colored. **d**, Changes in rotatable dihedral angles as a function of change in one of the rotatable dihedrals chosen arbitrarily as a control variable (solid and dashed curves correspond to the first and second solution sets, respectively). Simulation with our kinematic model produced seven curves that reflected the predicted range of configuration changes across which the structural integrity of the ring was preserved and only the value of the seven dihedral angles was altered. Dots correspond to dihedral angle values obtained from the ensemble of NMR structures, and triangles represent Rosetta predictions. The correlations predicted by our model correspond well to the distribution seen with NMR (20 candidate structures), supporting the hypothesis of 1-DOF motion for the cyclic peptides. However, some differences can be seen between the designed models and Rosetta predictions, which sampled a broader range of high-energy configurations.

permitted to deviate from ideal values. The larger cyclic peptides are somewhat more flexible than their smaller counterparts, however; this is likely because of the cumulative effect of the larger number of these slightly flexible degrees of freedom that were assumed to be fixed.

Our kinematic design method allows us to obtain all the dihedral angles (seven, as depicted in Fig. 1**c**) needed to create a controllable cyclic biomolecule given a candidate pattern of proline and non-proline amino acids. Additionally, it can predict the concerted motion of dihedral angles needed to maintain closure of the peptide. Fig. 1**d** depicts two solution sets derived for each cyclic peptide with the overlaid dihedral angles from the NMR structure candidates. Here, we randomly selected one of the seven rotatable dihedral angles as the control angle, and plotted the variation of the other six rotatable dihedral angles against the control angle. This shows our design method can determine the entire range of motion of cyclic peptides continously. Since the accessible conformational space is essentially one-dimensional for these peptides (unlike the extremely high-dimensional conformational spaces of proteins), this enables us to scan for the global energy minima for these peptides and make predictions about how these minima change in response to external stimuli, as will be discussed in the following section.

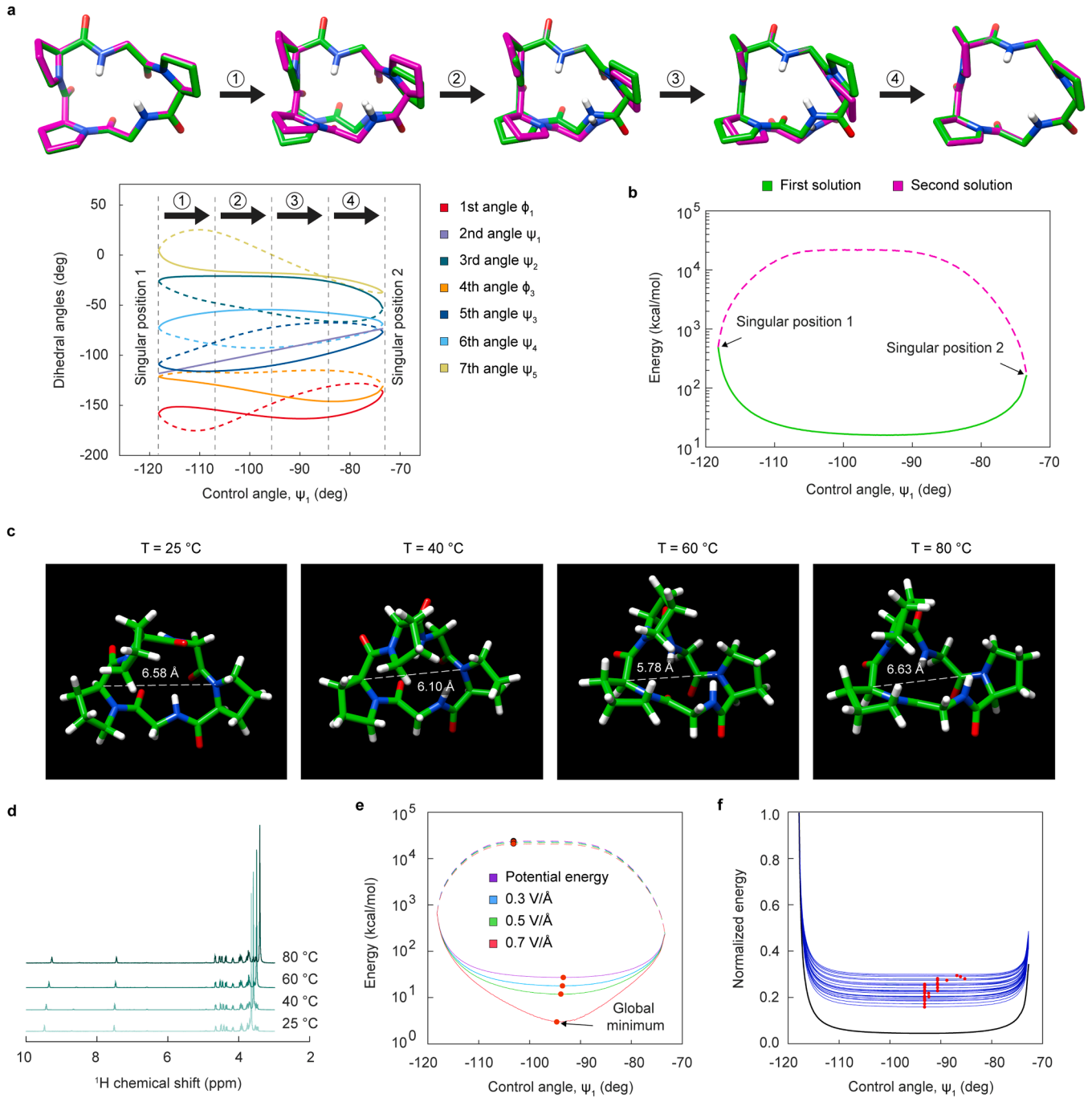

Fig. 2. Control mechanisms to manipulate the motions of cyclic peptide GPGPP. **a**, Full range of motion and singular positions for the GPGPP peptide. **b**, Energy profile for the complete motion of the GPGPP peptide. **c**, Molecular dynamics simulations of GPGPP at different temperatures. **d**, Temperature-dependent NMR for GPGPP at different temperatures. **e**, Energy curves for GPGPP in varying uniform electric fields (0.3, 0.5, and 0.7 V/Å) placed along the dipole moment of the molecule using a multipole power series expansion model. **f**, Varying energy curves for GPGPP (blue) in a non-uniform electric field with an externally charged particle (5×10^3 C) being shifted in the *xy*-plane at a fixed distance of 15 Å. Original energy curve is shown in black. Red dots show global energy minima.

Mechanisms to control the motions of cyclic peptides

Our strategy for building cyclic peptides is to design a simple mechanism with controllable motion along a single DOF. Our computational framework enables us to evaluate the energy profile along this DOF under the effect of different environmental conditions, permitting prediction of external perturbations that can alter the lowest-energy state in a desired way. Environmental parameters must be adjusted to find the optimum variation scenario for achieving the desired motion and function.

Fig. 2**a** presents the full range of motion of the class III GPGPP cyclic peptide. The two solution curves revealed by our kinetostatic method meet at two singular positions. In these positions, the control angle is no longer able to move the molecule and the mechanical advantage of the mechanism goes to zero. Using these solution curves, we can simulate the range of motion of the GPGPP peptide (Movie S1). To further investigate these singular positions, we determined the complete energy profile for the calculated solution curves (Fig. 2**b**). We observed that the singular positions contain either a very high or very low amount of energy, depending on the solution curve. For the first solution, the singularities are the maxima, whereas these positions are the minima for the second solution. This is in agreement with a longstanding perception in biology that stable molecular states are confined with reasonably large energetic barriers [140]. Therefore, we propose that these kinematic singular positions could be the reason for such large energy barriers, as they hinder molecular motion.

Supplementary material related to this article can be found online at doi:10.1016/j.nantod.2024.102247.

We ran molecular dynamics simulations to explore the conformational change of our designed macrocycles at different temperatures—and thereby assess whether temperature could be used to control molecular motion (see **Methods**; Fig. 2**c**). As predicted by our kinematic method, GPGPP does not undergo a large conformational change as temperatures changes, but rather a small change in internal diameter (~1 Å). This was further confirmed by temperature-dependent NMR spectra that did not show any signal collapse (Fig. 2**d**). We conclude that while temperature is not an effective means of controlling the conformation or motions of this peptide, its motions (and by extension, a function that could be engineered to depend on these motions) remain consistent across a range of temperatures.

In order to stimulate a biomolecule to go from one conformation to another, the morphology of the energy profile must somehow change to give rise to displacement of the global minimum (theoretically associated with the dominant conformational structure) in the energy profile along the axis (axes) associated with the conformational change of the molecule, and consequently to give motion to it. One possible way of to influencing influence peptide conformation is with an electric field, and we used two different models to examine potential impacts of uniform electric fields based on a charged-plate model and a multipole power series expansion model. A uniform electric field is one in which a molecule experiences the same intensity and direction of electric field lines regardless of the position of any of its atoms in space. This means that the electric field lines are both parallel and evenly spaced. We examined two ways to represent a uniform electric field and analyzed their application in the form of energy and force applied. Fig. 2**e** shows the simulated structural change of the GPGPP cyclic peptide under a variable electric field applied by two oppositely-charged plates. The curves represent the energy profile associated with the range of motion of the molecule under a given electric field condition, and the red dot indicates the location of the energetic minimum, and thus the favorable configuration. Changes in the electric field cause changes in the energy profile, and consequently, in the location of the global minimum. The changes in the conformation are subtle in this case. Non-uniform electric fields are more practical and realistic external field environments. Since all charged particles generate electric field lines, a simple charged particle in proximity to a molecule generates a non-uniform external electric field that interacts with that molecule. Fig. 2**f** shows one example of this scenario, where a charged particle (5×10^3 C) is shifted in the *xy*-plane at a fixed distance of 15 Å away from GPGPP. The results of these two models are not intended to conclusively prove that one model is superior, but simply to show how force field perturbations can be implemented for our controllable cyclic peptides. For the GPGPP peptide, which has a narrow range of mobility, we would expect shifts to be very small, but for larger and more flexible cyclic peptides, these models might show larger shifts in global minimum energy.

Supramolecular assemblies of the controllable cyclic peptides

The 1-DOF controllable cyclic peptides proposed here can be further combined to build supramolecular assemblies with more complex functions. These assemblies, which are loosely connected by hydrogen bonds, could move around, transport objects, and complete other tasks. This concept is reminiscent of "particle robots," [141] in which deterministic locomotion is a result of the stochastic radial movement (*i.e.,* oscillations) of many loosely-coupled, disc-shaped components, but on a much smaller scale.

Fig. 3**a** presents the assembled structure for different classes of controllable cyclic peptides (see the procedure in **Methods** and Movie S2). The five-residue peptides PPPGC and GPGPP form a unique sheet-like structure that is distinct from that of the other cyclic peptides. This interesting architecture is even noticeable at the microscale, as can be seen in scanning electron microscopy (SEM) images (Fig. 3**b**). In addition, SEM images of the CGPG peptide reveal hierarchical organization of needle-like crystals that are ~2 μm in diameter. This hierarchical arrangement suggests a controlled assembly process involving directed growth. Nucleation likely starts from specific molecular arrangements or nuclei, which then propagate into microneedles through a regulated growth mechanism. Peptide-peptide interactions, influenced by the specific structural features of the CGPG sequence, may contribute to the formation of these well-oriented microneedles. Growth kinetics and the interplay between intermolecular forces are crucial factors governing the hierarchical organization and growth of these assemblies. For the CGPG cyclic peptide in particular, hydrogen bonding might primarily involve interactions between backbone amide groups and carbonyl groups within the peptide chain. The side chains of the amino acids might also contribute to intra- and intermolecular hydrogen bonding interactions. Surprisingly, even after an extended incubation time (2 months), the structural features remained unchanged (Fig. S16), demonstrating the robustness and stability of the observed configurations.

Supplementary material related to this article can be found online at doi:10.1016/j.nantod.2024.102247.

PPPPPPP assemblies form spherical structures (Fig. 3**b**), indicating potential liquid-liquid phase separation during the early stages of self-assembly. In this proposed model, the solution separates into different liquid domains due to specific molecular interactions and local concentration variations. These separated phases subsequently evolve into the observed spherical formations as assembly progresses. In this scenario, nucleation and growth may involve the coalescence and evolution of these separated domains into defined structures. The repetition of proline residues in this 1-DOF construct might influence the hydrogen bonding capabilities within the cyclic peptide. As a secondary amine, proline might engage in hydrogen bonding interactions with adjacent peptide chains, primarily through its backbone amide and carbonyl groups. The resultant hydrogen bonding patterns could play a role in the observed formation of spherical structures during the early stages of self-assembly. Our observations align with recent studies [142,143] demonstrating similar assembly mechanisms in peptide systems.

To determine the supramolecular structure of the assembled cyclic peptides, we used circular dichroism (CD) and Fourier transform infrared (FTIR) spectroscopy. CD spectra showed negative bands at 218 nm and positive bands at 195 nm for PPPGC and GPGPP assemblies,

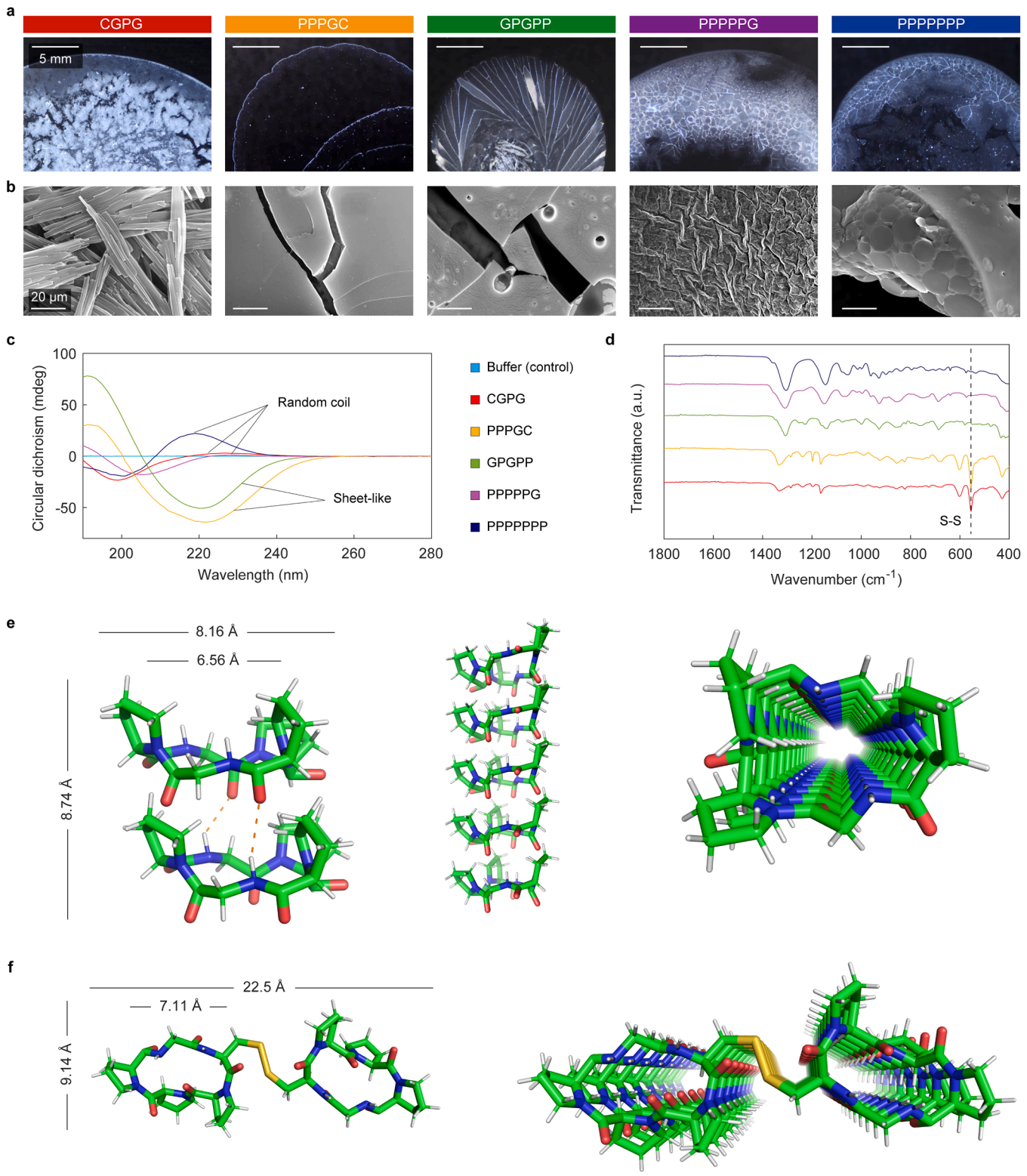

Fig. 3. Supramolecular assemblies of the controllable cyclic peptides. **a**, Light microscopic images of self-assembled structures formed by five different 1-DOF macrocycles. **b**, SEM micrographs of these same assemblies. **c**, Circular dichroism (CD) spectroscopy data collected for these assemblies at 25 °C. **d**, Fourier transform infrared (FTIR) spectra of the cyclic assemblies. **e**, **f**, Molecular structure of self-assembled (**e**) GPGPP and (**f**) PPPGC cyclic peptides based on CD and FTIR data. The models were constructed by manually docking an energy-minimized model of macrocycles until the hydrogen bonds were detected.

consistent with β-sheet structure (Fig. 3**c**) [144]. However, since these sequences possess only two hydrogen bond donors, the actual structure can only be sheet-like. The other assemblies showed very weak CD signal above 210 nm, with a negative band near 195 nm, representative of random coils [144]. FTIR spectra exhibited a sharp disulfide peak at 561 cm^{-1} for the cysteine-containing CGPG and PPPGC peptides; as expected, the other peptides do not show such a peak (Fig. 3**d**).

Based on the CD and FTIR data, we simulated the molecular structure

of GPGPP (Fig. 3**e**) and PPPGC (Fig. 3 **f**) assemblies arranged into nanotube structures through sheet-like hydrogen bonding. It should be noted that sheet-like assembly has been reported for other small cyclic peptides as well, which is consistent with our results [145–149]. Our models were constructed by manually docking an energy-minimized model of the macrocycles until hydrogen bonds were detected. The GPGPP assembly creates a continuous circular core (~6.5 Å in diameter) that can extend over millions of molecular units, a unique situation in biological materials. The PPPGC assembly forms two circular cores (~7 Å in diameter) due to disulfide bond formation. The most notable repetitive feature here is a set of β-sheets that are parallel to the long axis of the assembly, whereas the corresponding strands are perpendicular to this axis. These results indicate the stacking of distinctive units rather than β-strands, as is also suggested by the secondary structure analysis.

Our simulated molecular structures demonstrate that the self-assembly of PPPGC and GPGPP peptides into nanotubular structures is

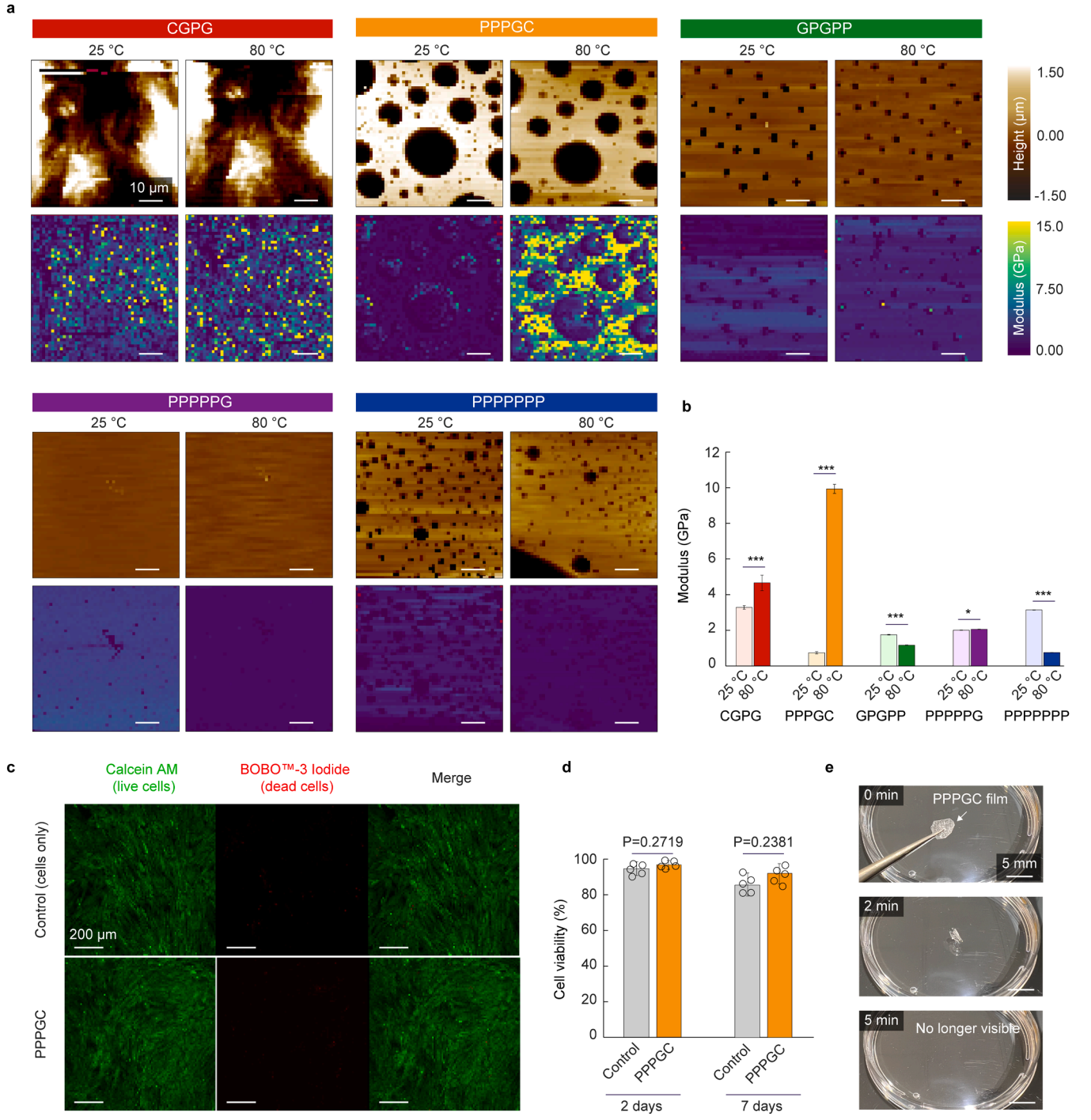

Fig. 4. Mechanical properties and biocompatibility of supramolecular biomaterials composed of controllable cyclic peptides. **a**, Atomic force microscopy (AFM)-derived height and calculated Young's modulus maps for cyclic peptide assemblies at 25 and 80 °C. **b**, Mean Young's modulus calculations from AFM indentation mapping (excluding pores), with standard error bars. **c**, *In vitro* biocompatibility of PPPGC film. Imaging of mouse adipose-derived stem cells (mADSC) incubated with or without PPPGC film at 37 °C for 7 days. Live cells are stained green (calcein AM) and dead cells are staind red (BOBO-3 iodide). **d**, Statistical analysis of the cell imaging assay data with two-ways ANOVA followed by Tukey's post-hoc analysis (n = 5). **e**, Images of degradation of a PPPGC film over time in 1X PBS buffer (pH 7.4) at 37 °C.

driven by the cooperative interplay of β-sheet hydrogen bonding and hydrophobic interactions. These peptides possess alternating proline and glycine residues in their cyclic form that promote the formation of β-sheets. Proline's rigid pyrrolidine ring restricts backbone flexibility, favoring extended conformations that are suitable for β-sheet assembly [150]. Additionally, the strategic positioning of proline residues every three or four positions introduces kinks in the polypeptide chain, facilitating the β-turn formation necessary for sheet closure [151]. Glycine's small size minimizes steric clashes, enabling tight packing of β-strands within the sheet. These β-sheets then stack upon each other, stabilized by intermolecular hydrogen bonding between carbonyl and amide groups, forming the observed nanotubular architectures [152].

Generating functional biocompatible/biodegradable supramolecular biomaterials from 1-DOF cyclic peptides

To explore the potential application of these controllable cyclic peptides as functional supramolecular biomaterials and study the macroscopic manifestation of the sheet-like structure of the PPPGC and GPGPP assemblies, we analyzed the mechanical properties of all the peptides using atomic force microscopy (AFM) imaging and indentation mapping (details in **Methods**). We acquired AFM height and calculated Young's modulus (E) data at two different temperatures, 25 °C and 80 °C (Fig. 4**a**). We could identify several trends that inform the material properties of these assemblies. For instance, mechanical properties are directly related to the size of the biomolecules, and we saw high modulus values for the small peptides CGPG and PPPGC, whereas the other peptides showed a very low modulus (Fig. 4**b**). Interactions between side-chain groups can further modulate the mechanical properties of these assemblies, and cysteine-containing assemblies showed very high modulus values because of strong disulfide bond formation. These disulfide bridges serve as stabilizing elements, reinforcing the interactions between individual peptide chains within the assembly [153]. This would also explain the notable differences between the equally-sized PPPGC and GPGPP peptides. Notably, the GPGPP assembly retains a stable β-sheet arrangement even at 80 °C, similar to PPPGC (Fig. S18). Consequently, highly organized assemblies of short cyclic peptides have a larger modulus than less organized assemblies composed of longer peptides. These observations suggest that the packing of shorter cysteine-containing cyclic peptides into sheet-like structures contributes to greater structural rigidity at high temperatures [154,155]. Indeed, the PPPGC assembly achieves a remarkably high modulus of 10 GPa at 80 °C, and we believe that the incorporation of cysteine contributes greatly to its higher-order structure, rigidity, and stability at elevated temperatures [156]. These AFM results indicate that even with short peptide sequences, one can modulate the characteristics of higher-order assemblies in a predictable manner through amino acid modification. The examination of thermodynamic and kinetic aspects of self-assembly places a particular emphasis on temperature-dependent, macroscopic changes in Gibbs free energy [157]. This analysis highlights the intricate balance between entropic and enthalpic contributions, a competition shaped by temperature variations within the system, which govern the fundamental aspects of peptide self-assembly. The PPPGC supramolecular structure is extremely stiff at 80 °C, with an E value comparable to the most rigid proteinaceous materials found in nature, such as silk (E = 1–10 GPa) [158,159], collagen (E = 1–9 GPa) [160,161], and keratin (E = 1.4–8 GPa) [162,163]. However, the unique advantage of PPPGC over these materials is that this modulus peaks at high temperatures, whereas other materials experience the inverse response to temperature. This could be highly advantageous for the design of rigid and stable biomaterials for sensing technology and stimulus-responsive soft materials.

We also examined the biocompatibility of PPPGC assemblies by imaging the effects of these films on the viability of mouse adipose-derived stem cells (mADSC). The mADSCs were seeded onto the films at 37 °C for 7 days, and stained with calcein AM to discriminate live cells based on intracellular esterase activity; dead cells were labeled with BOBO-3 Iodide, which detects the presence of nucleic acids in damaged membranes (Fig. 4**c**). The number of viable cells on PPPGC films was similar to that of the cells-only control, demonstrating that the film is not cytotoxic (Fig. 4**d**). Finally we conducted a degradation experiment to determine the functional lifetime of PPPGC film, and demonstrated the film self-degrades within five minutes in phosphate buffered saline (PBS) at 37 °C (Fig. 4**e**). This suggests that these structures must be encapsulated to achieve finer control over device degradation.

Conclusions

We present a design strategy for generating modular controllable 1-DOF cyclic peptides with programmed one-dimensional motions. These peptides have major advantages over other nanoscale cyclic structures, including sub-nanometer control over the internal diameter, and the potential to control internal and external chemical functionality under different external stimuli. We studied the self-assembly of these cyclic peptides and determined that PPPGC- and GPGPP-based assemblies form nanotube-like structures through β-sheet hydrogen bonding. Moreover, the presence of cysteine in PPPGC creates a higher-order structure with remarkable rigidity and stability at high temperatures, with a Young's modulus of 10 GPa at 80 °C—comparable to the most rigid proteinaceous materials in nature, such as silk, collagen and keratin. Unlike these materials, however, our PPPGC assembly demonstrates a direct relation with temperature which makes it suitable for the development of unique functional, biocompatible, and biodegradable supramolecular biomaterials.

While our study highlights the promising attributes of ultra-confined, controllable cyclic peptide assemblies as biomaterials, challenges remain that could hinder their broader application. Scalability and cost-effectiveness could be potential challenges, as the specific synthesis techniques involved in creating these assemblies may not be compatible with large-scale production. Furthermore, integrating these cyclic peptides assemblies with other materials or existing biomedical technologies might pose compatibility issues that require further exploration. Overcoming these challenges might necessitate advancements in synthetic biology to enable more efficient and cost-effective synthesis methods, as well as deeper investigations into compatibility with other biomaterials.

In summary, this study explores the self-assembly behaviors and structural characteristics of ultra-confined cyclic peptides, revealing their remarkable stability, intricate high-order structures, and fascinating mechanical properties. The insights pertaining to their structure-property relationships lay the groundwork for the rational design of novel peptide-based materials tailored to achieve specific functionalities, and the ongoing exploration of these peptide assemblies could open new avenues for practical applications in a wide range of domains including reconfigurable nanomaterials, stimuli-responsive biomaterials, and thermally stable nanosheets.

Methods

Peptide synthesis

Peptides were synthesized using standard Fmoc solid phase peptide synthesis (SPPS) on preloaded 2-chlorotrityl chloride resin. After the final Fmoc deprotection, the resin-bound linear peptide was treated with 2% (v/v) hydrazine monohydrate in dimethylformamide (DMF, Sigma-Aldrich, anhydrous, ≥99.9%) to remove the C-terminal protecting group. Subsequently, the N- and C-termini were coupled in a liquid-phase coupling reaction performed after cleaving the protected linear peptide from the resin. Crude peptides were purified using an Agilent Infinity Preparative HPLC to more than 98%, as verified by HPLC followed by mass spectrometry confirmation of their identity (Supplementary Fig. S7–S11). Details of the synthesis process in provided in

Supplementary Note S2. All peptides were stored at −80 °C.

Kinetostatic design

Cyclic peptides are modeled as kinematic chains, which is a common method in protein design and protein folding [164]. The DOF of a chain could be determined using Grübler–Kutzbach criterion. Zero-position notation was used to characterize the links and joints of the polypeptide chain, where all vectors for joint axes and directions were defined by a single-base coordinate system with a chosen point of origin, or zero-position. The zero-position acts as our reference point from which we extend the position of the next link in the kinematic linkage, successively applying the next dihedral angle in the chain to calculate the next link position. To convert the open-loop peptide chain to a closed-loop macrocycle, the last link (end effector) must be positioned and oriented at the base of the first link. Analytically, this results in a system of nonlinear equations referred to as loop-closure equations. Zero-position formulation yields 12 equations with 7 unknowns. To solve this system of nonlinear equations, we utilized the MATLAB unconstrained nonlinear system solver, fminunc. Further details of the kinetostatic method and electric field excitations are presented in **Supplementary Note S1**.

Rosetta modeling

We used the Rosetta simple_cycpep_predict application [164,165], to sample conformations and predict structures of cyclic peptides CGPG, PPPGC, GPGPP, PPPPPG, and PPPPPPP. Like Protofold [166], Rosetta uses robotics-inspired kinematic closure methods to sample closed conformations of peptides. However, where the initial design methods using Protofold solved for exactly seven degrees of backbone conformational freedom, keeping all constrained degrees of freedom at ideal values, Rosetta is able to sample more broadly. Since smaller cyclic peptides are often strained, we added support for sampling small deviations from ideal bond lengths and bond angles, as described in **Supplementary Note S3**. We carried out simulations with torsion-space relaxation of sampled conformations (in which bond angles and bond lengths were fixed to their sampled values), and with and without a final round of Cartesian-space relaxation (in which bond angles and bond lengths were permitted to change during relaxation). The Rosetta ref2015 and ref2015_cart energy functions [167] were used for torsion-space and Cartesian-space relaxations, respectively, and for final scoring. All predictions were carried out blindly, without knowledge of the initial design models or of NMR structures when available. Full details and instructions for reproducing these simulations are in **Supplementary Note S3**.

NMR spectroscopy

Each cyclic peptide was dissolved at concentrations of ~5 mg/ml in dimethyl sulfoxide-d6 (Sigma-Aldrich). NMR data were collected on a Bruker AVANCE 500 MHz or Varian INOVA 600 MHz spectrometer equipped with a triple-resonance (^{1}H, ^{13}C, ^{15}N) inverse cryogenic probe. Resonance assignments were obtained using standard procedures. Data were processed in TOPSPIN v 3.5 (Bruker) and analyzed in Sparky or CCPN NMR Analysis v2.5. Structures were calculated in CNS (Crystallography & NMR System). The preliminary structures were calculated in Cyana followed by refinement in CNS. For temperature-dependent NMR, data were also collected at 40, 60, and 80 °C.

Molecular dynamics (MD) simulations

MD simulations were performed using the NAMD [168] and CHARMM22 force field [169]. The cut-off distance for van der Waals interactions was set to 12 Å. The whole system was heated from 0 K to 298.15 K, 313.15 K, 333.15 K, and 353.15 K over a 62-ps simulation using weakly-coupled Langevin dynamics, and the target temperature was then maintained. Pressure was maintained at 1 atm using a Langevin piston Nose-Hoover barostat (with a piston period of 100 fs and a decay time of 50 fs). The LINCS algorithm was applied at each step to preserve bond lengths. The temperature and volume of each system were equilibrated by running 400 ps of constant-volume, constant-temperature (NVT) simulation, followed by 400 ps of constant-pressure, constant-temperature (NPT) simulations. Production runs in the NPT ensemble were then conducted for 20 ns.

Self-assembly process of the cyclic peptide

Peptides were dissolved in 2 mM phosphate buffer (Alfa Aesar) at pH 8.0 at a concentration of 5 mg/ml. The samples were incubated at 20 °C for five days with frequent shaking before examination.

Scanning electron microscopy

Peptides were dissolved in 2 mM phosphate buffer at pH 8.0 at a concentration of 5 mg/ml. Samples were incubated at 20 °C for five days with frequent shaking before examination. A 5 μl aliquot was allowed to dry on a microscope glass coverslip under ambient conditions overnight and sputter-coated with Au/Pd (5 nm thickness) using a sputter coater (CCU-010, Safematic). The samples were then imaged using a Verios 460 L SEM at 15 keV and 2500X magnification. Data collection and analysis were carried out with xT microscope Control software.

Circular dichroism spectroscopy

CD spectra were recorded on an Applied Photophysics Pi-Star 180 spectropolarimeter (Surrey, UK) using a 1-mm path-length cuvette with 3 mg of peptide in 2 mM sodium phosphate buffer. Wavelength scans were collected between 190 and 280 nm using a 2 nm bandwidth, 2 nm step size, and 30 s/point data averaging for a total scan time of ~15 min.

Fourier transform infrared spectroscopy

FTIR spectra were acquired with a Nicolet Magna 560 (Thermo Fisher Scientific) and attenuated total reflectance (ATR) ZnSe. The samples were cast directly onto the ATR crystal. Measurements were performed and analyzed at several areas. Prior to each experiment, the diamond lens was cleaned using acetone, followed by deionized water. The FTIR spectra were background subtracted and baseline corrected with OMNIC software v.8.3.103.

Atomic force microscopy

Peptides were dissolved in 2 mM phosphate buffer, pH 8.0 at a concentration of 5 mg/ml. The samples were incubated at 20 °C for five days with frequent shaking before examination. AFM images were taken by depositing 5 μl solutions onto freshly cleaved V1 grade mica (Ted Pella). Modulus maps were generated using an MFP-3D-Bio Atomic Force Microscope (Oxford Instruments Asylum Research) and an AC-160 probes (Olympus) [170]. Heights and forces were measured simultaneously during indentation over a 50 ×50 array of locations equally spaced across a 50 ×50 μm^2 area, for a total of 2500 force curves per map. Each force curve was measured with 2 μm/s approach and retraction velocities and 5 μN trigger force (max load). All samples were first studied at room temperature, then a PolyHeater accessory (Oxford Instruments Asylum Research) was energized for *in situ* heating to 80 °C. The system was allowed to stabilize for 10 minutes, and indentation arrays were then re-acquired. The modulus for each indentation curve was calculated using the punch indentation model with a contact radius of 50 nm and assumed sample Poisson ratio of 0.33. Finally, masks were generated from each respective height map in order to remove any extraneous measurements from within the topographic pores (where

indentation measurements are prone to artifacts from the substrate or edge effects). This was achieved using a simple height threshold based on the plane of the assembled cyclic peptides, thus excluding measurements from lower depths (*i.e.,* in pores). Occasional indentations do not result in physically reasonable fits as well and are thus also removed from further analysis (< 2.2% of all measurements). Final error bars in Fig. 4**b** indicate the resulting standard error for each modulus map, based on N values ranging from 1525 individual measurements (for the most porous specimen, the PPPGC, which is 61% smooth film and 39% pores) to nearly 100% of the 2500 distinct indentations at each temperature per specimen.

Cell imaging assay

Mouse adipose-derived stem cells (mADSC, iXCells Biotechnologies) were cultured in Dulbecco's Modified Eagle's Medium supplemented (Gibco) with 10% fetal bovine serum (Gibco) and 1% penicillin-streptomycin (Gibco) at 37°C and 5% CO2. At 80–90% confluence of passage 4, the cells were detached from the flasks using trypsin/EDTA (Gibco) and seeded onto PPPGC films at a density of 5×10^6 cells/ml. After seven days, the cells were stained with a LIVE/DEAD cell imaging kit (Invitrogen) and imaged with a Leica SP8 confocal laser microscope with excitation/emission at 488 nm/515 nm and 570 nm/602 nm.

Film degradation assay

PPPGC peptide was dissolved in 2 mM phosphate buffer (Alfa Aesar) at pH 8.0 at a concentration of 5 mg/ml. The sample was incubated at 20 °C for five days with frequent shaking before examination. A 20 µl aliquot was allowed to dry on a microscope glass coverslip under ambient conditions overnight and later carefully removed using a tweezer. The PPPGC film was placed in a glass dish filled with 5 ml of PBS (Gibco, pH 7.4) for degradation at room temperature.

CRediT authorship contribution statement

Alexandra Pozhidaeva: Data curation, Formal analysis, Investigation, Methodology, Writing – original draft. **Horea Ilies:** Conceptualization, Funding acquisition, Investigation, Project administration, Resources, Supervision, Writing – original draft, Writing – review & editing. **Will Linthicum:** Data curation, Formal analysis, Methodology, Visualization, Writing – original draft. **Kazem Kazerounian:** Conceptualization, Formal analysis, Funding acquisition, Project administration, Resources, Supervision, Writing – original draft, Writing – review & editing. **Meysam Chorsi:** Conceptualization, Data curation, Formal analysis, Investigation, Methodology, Project administration, Resources, Software, Validation, Visualization, Writing – original draft, Writing – review & editing. **Thanh D. Nguyen:** Investigation, Resources, Supervision, Writing – original draft. **Bryan D. Huey:** Data curation, Formal analysis, Investigation, Methodology, Resources, Software, Supervision, Writing – original draft. **Jeffrey Hoch:** Funding acquisition, Resources, Supervision. **Olga Vinogradova:** Data curation, Methodology, Supervision, Writing – original draft. **Vitaliy Gorbatyuk:** Data curation, Investigation, Methodology. **Pouya Tavousi:** Data curation, Formal analysis, Methodology. **Vikram Khipple Mulligan:** Data curation, Formal analysis, Methodology, Software, Writing – original draft, Writing – review & editing. **H. Tom Soh:** Supervision, Writing – review & editing. **Caitlyn Mundrane:** Data curation, Formal analysis, Methodology, Software, Writing – original draft. **Yihang Chen:** Data curation, Methodology.

Declaration of Competing Interest

The authors declare the following financial interests/personal relationships which may be considered as potential competing interests. Thanh D. Nguyen has a conflict of interest with the companies of SingleTImeMicroneedles (STM) Inc. and PiezoBioMembrane (PBM) Inc. Vikram Khipple Mulligan is a co-founder of Menten AI, a biotechnology company. Horea Ilies reports financial support was provided by University of Connecticut. Horea Ilies reports a relationship with University of Connecticut that includes: funding grants

Data Availability

Data will be made available on request.

Acknowledgements

This research is funded by the National Science Foundation (grant No. 1635103). A.P. and J.C.H. are supported by grant P41GM111135 from the US National Institutes of Health. V.K.M. was funded by the Simons Foundation .

Author contributions

M.T.C., K.K., and H.I. conceived the idea and designed the project. M. T.C., W.L., and C.M. designed the experiments. V.K.M. performed computational Rosetta simulations. M.T.C., W.L., C.M., A.P., Y.C., P.T., V.G., and O.V. fabricated the samples and performed the measurements. J.H., B.D.H., T.D.N., H.T.S., K.K., and H.I. guided the investigations, offered experimental insights, and provided professional evaluation of the results. All authors contributed to discussions and manuscript writing.

Appendix A. Supporting information

Supplementary data associated with this article can be found in the online version at doi:10.1016/j.nantod.2024.102247.

References

[1] R. Langer, Controlling the movement of molecules, Q. Rev. Biophys. 52 (2019).
[2] Y. Yuan, et al., Chaperonin-GroEL as a smart hydrophobic drug delivery and tumor targeting molecular machine for tumor therapy, Nano Lett. 18 (2018) 921–928.
[3] C.-A. Cheng, T. Deng, F.-C. Lin, Y. Cai, J.I. Zink, Supramolecular nanomachines as stimuli-responsive gatekeepers on mesoporous silica nanoparticles for antibiotic and cancer drug delivery, Theranostics 9 (2019) 3341.
[4] W. Chen, C.A. Glackin, M.A. Horwitz, J.I. Zink, Nanomachines and other caps on mesoporous silica nanoparticles for drug delivery, Acc. Chem. Res. 52 (2019) 1531–1542.
[5] S. Biswas, et al., Biomolecular robotics for chemomechanically driven guest delivery fuelled by intracellular ATP, Nat. Chem. 5 (2013) 613–620.
[6] A.J. Ben-Sasson, et al., Design of biologically active binary protein 2D materials, Nature 589 (2021) 468–473.
[7] E. Moulin, L. Faour, C.C. Carmona-Vargas, N. Giuseppone, From molecular machines to stimuli-responsive materials, Adv. Mater. 32 (2020) 1906036.
[8] U. Saha, K. Todi, B.D. Malhotra, Emerging DNA-based multifunctional nanobiomaterials towards electrochemical sensing applications, Nanoscale 13 (2021) 10305–10319.
[9] C. Xue, et al., Stimuli-responsive autonomous-motion molecular machine for sensitive simultaneous fluorescence imaging of intracellular microRNAs, Anal. Chem. 93 (2021) 9869–9877.
[10] M. Baroncini, et al., Making and operating molecular machines: a multidisciplinary challenge, ChemistryOpen 7 (2018) 169–179.
[11] R. Eelkema, et al., Nanomotor rotates microscale objects, 163-163, Nature 440 (2006), 163-163.
[12] P. Štacko, et al., Locked synchronous rotor motion in a molecular motor, Science 356 (2017) 964–968.
[13] S. Konermann, et al., Optical control of mammalian endogenous transcription and epigenetic states, Nature 500 (2013) 472–476.
[14] F. Ran, et al., Genome engineering using the CRISPR-Cas9 system, Nat. Protoc. 8 (2013) 2281–2308.
[15] D.A. Leigh, J.K. Wong, F. Dehez, F. Zerbetto, Unidirectional rotation in a mechanically interlocked molecular rotor, Nature 424 (2003) 174–179.
[16] A.M. Brouwer, et al., Photoinduction of fast, reversible translational motion in a hydrogen-bonded molecular shuttle, Science 291 (2001) 2124–2128.
[17] V. Serreli, C.-F. Lee, E.R. Kay, D.A. Leigh, A molecular information ratchet, Nature 445 (2007) 523–527.

[18] S. Corra, et al., Kinetic and energetic insights into the dissipative non-equilibrium operation of an autonomous light-powered supramolecular pump, Nat. Nanotechnol. 17 (2022) 746–751.
[19] H. Huang, T. Aida, Towards molecular motors in unison, 407-407, Nat. Nanotechnol. 14 (2019), https://doi.org/10.1038/s41565-019-0414-1, 407-407.
[20] T. Kudernac, et al., Tuning the temperature dependence for switching in dithienylethene photochromic switches, J. Phys. Chem. A 117 (2013) 8222–8229.
[21] S. Erbas-Cakmak, D.A. Leigh, C.T. McTernan, A.L. Nussbaumer, Artificial molecular machines, Chem. Rev. 115 (2015) 10081–10206.
[22] G. Storch, O. Trapp, Temperature-controlled bidirectional enantioselectivity in a dynamic catalyst for asymmetric hydrogenation, Angew. Chem. Int. Ed. 54 (2015) 3580–3586.
[23] J. Boekhoven, et al., Dissipative self-assembly of a molecular gelator by using a chemical fuel, Angew. Chem. 122 (2010) 4935–4938.
[24] N. Koumura, E.M. Geertsema, A. Meetsma, B.L. Feringa, Light-driven molecular rotor: Unidirectional rotation controlled by a single stereogenic center, J. Am. Chem. Soc. 122 (2000) 12005–12006.
[25] J.T. Foy, et al., Dual-light control of nanomachines that integrate motor and modulator subunits, Nat. Nanotechnol. 12 (2017) 540–545.
[26] J. Valero, N. Pal, S. Dhakal, N.G. Walter, M. Famulok, A bio-hybrid DNA rotor–stator nanoengine that moves along predefined tracks, Nat. Nanotechnol. 13 (2018) 496–503.
[27] Dunn, J. & Grider, M. Physiology, adenosine triphosphate (ATP). (2020).
[28] T. Kudernac, et al., Electrically driven directional motion of a four-wheeled molecule on a metal surface, Nature 479 (2011) 208–211.
[29] Y. Zhang, et al., Simultaneous and coordinated rotational switching of all molecular rotors in a network, Nat. Nanotechnol. 11 (2016) 706–712.
[30] E. Kopperger, et al., A self-assembled nanoscale robotic arm controlled by electric fields, Science 359 (2018) 296–301.
[31] L. Zhang, et al., An electric molecular motor, Nature 613 (2023) 280–286.
[32] V. García-López, et al., Molecular machines open cell membranes, Nature 548 (2017) 567–572.
[33] Y. Zhang, et al., A chiral molecular propeller designed for unidirectional rotations on a surface, Nat. Commun. 10 (2019) 1–9.
[34] B. Esteban-Fernández de Ávila, et al., Hybrid biomembrane–functionalized nanorobots for concurrent removal of pathogenic bacteria and toxins, Sci. Robot. 3 (2018) eaat0485.
[35] M. Calvaresi, et al., Mechanical tightening of a synthetic molecular knot, Chem 9 (2023) 65–75.
[36] S. Can, S. Lacey, M. Gur, A.P. Carter, A. Yildiz, Directionality of dynein is controlled by the angle and length of its stalk, Nature 566 (2019) 407–410.
[37] B. Yurke, A.J. Turberfield, A.P. Mills, F.C. Simmel, J.L. Neumann, A DNA-fuelled molecular machine made of DNA (https://doi.org:), Nature 406 (2000) 605–608, https://doi.org/10.1038/35020524.
[38] M. Vogt, et al., Storage of mechanical energy in DNA nanorobotics using molecular torsion springs. *Nature*, Physics (2023) 1–11.
[39] J. Kim, F.C. Simmel, Scaling up genelet circuits, Nat. Chem. 14 (2022) 1210–1211.
[40] A.-K. Pumm, et al., A DNA origami rotary ratchet motor, Nature 607 (2022) 492–498.
[41] T.-G. Cha, et al., A synthetic DNA motor that transports nanoparticles along carbon nanotubes (https://doi.org:), Nat. Nanotechnol. 9 (2014) 39–43, https://doi.org/10.1038/nnano.2013.257.
[42] X. Shi, et al., Sustained unidirectional rotation of a self-organized DNA rotor on a nanopore, Nat. Phys. 18 (2022) 1105–1111.
[43] K. Sakakibara, T. Fujisawa, J.P. Hill, K. Ariga, Conformational interchange of a carbohydrate by mechanical compression at the air–water interface, Phys. Chem. Chem. Phys. 16 (2014) 10286–10294.
[44] F. Coutrot, C. Romuald, E. Busseron, A new pH-switchable dimannosyl [c2] daisy chain molecular machine, Org. Lett. 10 (2008) 3741–3744.
[45] B.-B. Ke, L.-S. Wan, Z.-K. Xu, Controllable construction of carbohydrate microarrays by site-directed grafting on self-organized porous films (https://doi.org:), Langmuir 26 (2010) 8946–8952, https://doi.org/10.1021/la904729b.
[46] A. Brito, et al., Carbohydrate amphiphiles for supramolecular biomaterials: Design, self-assembly, and applications, Chem 7 (2021) 2943–2964.
[47] X. Hou, T. Zaks, R. Langer, Y. Dong, Lipid nanoparticles for mRNA delivery (https://doi.org:), Nat. Rev. Mater. 6 (2021) 1078–1094, https://doi.org/10.1038/s41578-021-00358-0.
[48] X. Wang, et al., Preparation of selective organ-targeting (SORT) lipid nanoparticles (LNPs) using multiple technical methods for tissue-specific mRNA delivery (https://doi.org:), Nat. Protoc. 18 (2023) 265–291, https://doi.org/10.1038/s41596-022-00755-x.
[49] B.B. Mendes, et al., Nanodelivery of nucleic acids (https://doi.org:), Nat. Rev. Methods Prim. 2 (2022) 24, https://doi.org/10.1038/s43586-022-00104-y.
[50] Q. Shi, et al., Digital micelles of encoded polymeric amphiphiles for direct sequence reading and ex vivo label-free quantification (https://doi.org:), Nat. Chem. 15 (2023) 257–270, https://doi.org/10.1038/s41557-022-01076-y.
[51] L. Mahadevan, P. Matsudaira, Motility powered by supramolecular springs and ratchets (https://doi.org:), Science 288 (2000) 95–99, https://doi.org/10.1126/science.288.5463.95.
[52] G.R. Mali, et al., Shulin packages axonemal outer dynein arms for ciliary targeting, Science 371 (2021) 910–916.
[53] J. Liu, et al., Light-induced control of protein destruction by opto-PROTAC (https://doi.org:), Sci. Adv. 6 (2020) eaay5154, https://doi.org/10.1126/sciadv.aay5154.
[54] S.E. Cason, E.L. Holzbaur, Selective motor activation in organelle transport along axons, Nat. Rev. Mol. Cell Biol. 23 (2022) 699–714.
[55] J.P. Bravo, et al., Structural basis for mismatch surveillance by CRISPR–Cas9, Nature 603 (2022) 343–347.
[56] M.M. Elshenawy, et al., Lis1 activates dynein motility by modulating its pairing with dynactin, Nat. Cell Biol. 22 (2020) 570–578.
[57] H. Jia, et al., 3D printed protein-based robotic structures actuated by molecular motor assemblies, Nat. Mater. 21 (2022) 703–709.
[58] H.T. Hsueh, et al., Machine learning-driven multifunctional peptide engineering for sustained ocular drug delivery (https://doi.org:), Nat. Commun. 14 (2023) 2509, https://doi.org/10.1038/s41467-023-38056-w.
[59] T.D. Brown, K.A. Whitehead, S. Mitragotri, Materials for oral delivery of proteins and peptides (https://doi.org:), Nat. Rev. Mater. 5 (2020) 127–148, https://doi.org/10.1038/s41578-019-0156-6.
[60] A. Capecchi, et al., Machine learning designs non-hemolytic antimicrobial peptides, Chem. Sci. 12 (2021) 9221–9232.
[61] G. De Bo, et al., An artificial molecular machine that builds an asymmetric catalyst (https://doi.org:), Nat. Nanotechnol. 13 (2018) 381–385, https://doi.org/10.1038/s41565-018-0105-3.
[62] L. van Dijk, et al., Molecular machines for catalysis (https://doi.org:), Nat. Rev. Chem. 2 (2018) 0117, https://doi.org/10.1038/s41570-018-0117.
[63] L. Zhang, V. Marcos, D.A. Leigh, Molecular machines with bio-inspired mechanisms (https://doi.org:), Proc. Natl. Acad. Sci. 115 (2018) 9397–9404, https://doi.org/10.1073/pnas.1712788115.
[64] M.T. Chorsi, et al., Highly piezoelectric, biodegradable, and flexible amino acid nanofibers for medical applications, Sci. Adv. 9 (2023) eadg6075.
[65] M. Muttenthaler, G.F. King, D.J. Adams, P.F. Alewood, Trends in peptide drug discovery (https://doi.org:), Nat. Rev. Drug Discov. 20 (2021) 309–325, https://doi.org/10.1038/s41573-020-00135-8.
[66] N. Mookherjee, M.A. Anderson, H.P. Haagsman, D.J. Davidson, Antimicrobial host defence peptides: functions and clinical potential (https://doi.org:), Nat. Rev. Drug Discov. 19 (2020) 311–332, https://doi.org/10.1038/s41573-019-0058-8.
[67] R.E.W. Hancock, H.-G. Sahl, Antimicrobial and host-defense peptides as new anti-infective therapeutic strategies (https://doi.org:), Nat. Biotechnol. 24 (2006) 1551–1557, https://doi.org/10.1038/nbt1267.
[68] M.J. Webber, E.A. Appel, E.W. Meijer, R. Langer, Supramolecular biomaterials (https://doi.org:), Nat. Mater. 15 (2016) 13–26, https://doi.org/10.1038/nmat4474.
[69] T. Aida, E. Meijer, S. Stupp, Functional supramolecular polymers, Science 335 (2012) 813–817.
[70] M.L. Ślęczkowski, M.F. Mabesoone, P. Ślęczkowski, A.R. Palmans, E. Meijer, Competition between chiral solvents and chiral monomers in the helical bias of supramolecular polymers, Nat. Chem. 13 (2021) 200–207.
[71] S.P. Wijnands, W. Engelen, R.P. Lafleur, E. Meijer, M. Merkx, Controlling protein activity by dynamic recruitment on a supramolecular polymer platform, Nat. Commun. 9 (2018) 65.
[72] E.A. Appel, J. del Barrio, X.J. Loh, O.A. Scherman, Supramolecular polymeric hydrogels, Chem. Soc. Rev. 41 (2012) 6195–6214.
[73] Z. Chen, et al., Solvent-free autocatalytic supramolecular polymerization, Nat. Mater. 21 (2022) 253–261.
[74] Y.S. Kim, et al., Thermoresponsive actuation enabled by permittivity switching in an electrostatically anisotropic hydrogel, Nat. Mater. 14 (2015) 1002–1007.
[75] H. Qi, et al., DNA-directed self-assembly of shape-controlled hydrogels (https://doi.org:), Nat. Commun. 4 (2013) 2275, https://doi.org/10.1038/ncomms3275.
[76] S. Häkkinen, et al., Polymerisation-induced self-assembly of graft copolymers (https://doi.org:), Angew. Chem. Int. Ed. 61 (2022) e202210518, https://doi.org/10.1002/anie.202210518.
[77] van Son, M.H. *et al.* Highly Ordered Supramolecular Materials of Phase-Separated Block Molecules for Long-Range Exciton Transport. *Advanced Materials*, 2300891.
[78] E. Weyandt, et al., Controlling the length of porphyrin supramolecular polymers via coupled equilibria and dilution-induced supramolecular polymerization, Nat. Commun. 13 (2022) 248.
[79] S.I. Hendrikse, et al., Controlling and tuning the dynamic nature of supramolecular polymers in aqueous solutions, Chem. Commun. 53 (2017) 2279–2282.
[80] R. Freeman, et al., Reversible self-assembly of superstructured networks (https://doi.org:), Science 362 (2018) 808–813, https://doi.org/10.1126/science.aat6141.
[81] J. Zhang, et al., Self-assembly and disassembly of stimuli responsive tadpole-like single chain nanoparticles using a switchable hydrophilic/hydrophobic boronic acid cross-linker, Polym. Chem. 8 (2017) 4079–4087.
[82] N. Sasaki, et al., Supramolecular double-stranded Archimedean spirals and concentric toroids, Nat. Commun. 11 (2020) 3578.
[83] X. Lou, et al., Dynamic diversity of synthetic supramolecular polymers in water as revealed by hydrogen/deuterium exchange, Nat. Commun. 8 (2017) 15420.
[84] P.A. Guerette, et al., Accelerating the design of biomimetic materials by integrating RNA-seq with proteomics and materials science (https://doi.org:), Nat. Biotechnol. 31 (2013) 908–915, https://doi.org/10.1038/nbt.2671.
[85] E.A. Appel, et al., Ultrahigh-water-content supramolecular hydrogels exhibiting multistimuli responsiveness, J. Am. Chem. Soc. 134 (2012) 11767–11773.
[86] R. Pugliese, F. Gelain, Characterization of elastic, thermo-responsive, self-healable supramolecular hydrogel made of self-assembly peptides and guar gum, Mater. Des. 186 (2020) 108370.
[87] A.S. Carlini, W. Choi, N.C. McCallum, N.C. Gianneschi, pH-responsive charge-conversion progelator peptides, Adv. Funct. Mater. 31 (2021) 2007733.

[88] S. Zhang, et al., A pH-responsive supramolecular polymer gel as an enteric elastomer for use in gastric devices (https://doi.org:), Nat. Mater. 14 (2015) 1065–1071, https://doi.org/10.1038/nmat4355.
[89] Y. Yu, et al., Oligosaccharides self-assemble and show intrinsic optical properties, J. Am. Chem. Soc. 141 (2019) 4833–4838.
[90] Q. Zhang, D.H. Qu, H. Tian, Photo-regulated supramolecular polymers: shining beyond disassembly and reassembly, Adv. Opt. Mater. 7 (2019) 1900033.
[91] J.D. Tovar, Supramolecular construction of optoelectronic biomaterials, Acc. Chem. Res. 46 (2013) 1527–1537.
[92] A.K. Gaharwar, I. Singh, A. Khademhosseini, Engineered biomaterials for in situ tissue regeneration (https://doi.org:), Nat. Rev. Mater. 5 (2020) 686–705, https://doi.org/10.1038/s41578-020-0209-x.
[93] M.P. Lutolf, J.A. Hubbell, Synthetic biomaterials as instructive extracellular microenvironments for morphogenesis in tissue engineering (https://doi.org:), Nat. Biotechnol. 23 (2005) 47–55, https://doi.org/10.1038/nbt1055.
[94] E.A. Appel, et al., Self-assembled hydrogels utilizing polymer–nanoparticle interactions, Nat. Commun. 6 (2015) 6295.
[95] M.R. Prausnitz, R. Langer, Transdermal drug delivery (https://doi.org:), Nat. Biotechnol. 26 (2008) 1261–1268, https://doi.org/10.1038/nbt.1504.
[96] F. Wang, et al., Tumour sensitization via the extended intratumoural release of a STING agonist and camptothecin from a self-assembled hydrogel (https://doi.org:), Nat. Biomed. Eng. 4 (2020) 1090–1101, https://doi.org/10.1038/s41551-020-0597-7.
[97] S.H. Jeong, M. Kim, T.Y. Kim, H. Choi, S.K. Hahn, Biomimetic supramolecular drug delivery hydrogels for accelerated skin tissue regeneration (https://doi.org:), ACS Biomater. Sci. Eng. 7 (2021) 4581–4590, https://doi.org/10.1021/acsbiomaterials.1c00705.
[98] R.N. Shah, et al., Supramolecular design of self-assembling nanofibers for cartilage regeneration (https://doi.org:), Proc. Natl. Acad. Sci. 107 (2010) 3293–3298, https://doi.org/10.1073/pnas.0906501107.
[99] W. Ji, et al., Rigid tightly packed amino acid crystals as functional supramolecular materials (https://doi.org:), ACS Nano 13 (2019) 14477–14485, https://doi.org/10.1021/acsnano.9b08217.
[100] S. Koutsopoulos, S. Zhang, Long-term three-dimensional neural tissue cultures in functionalized self-assembling peptide hydrogels, matrigel and collagen I, Acta Biomater. 9 (2013) 5162–5169.
[101] S. Koutsopoulos, S. Zhang, Two-layered injectable self-assembling peptide scaffold hydrogels for long-term sustained release of human antibodies, J. Control. Release 160 (2012) 451–458.
[102] K. Sato, M.P. Hendricks, L.C. Palmer, S.I. Stupp, Peptide supramolecular materials for therapeutics (https://doi.org:), Chem. Soc. Rev. 47 (2018) 7539–7551, https://doi.org/10.1039/c7cs00735c.
[103] M.P. Hendricks, K. Sato, L.C. Palmer, S.I. Stupp, Supramolecular Assembly of Peptide Amphiphiles (https://doi.org:), Acc. Chem. Res. 50 (2017) 2440–2448, https://doi.org/10.1021/acs.accounts.7b00297.
[104] Y. Shen, et al., Chiral self-assembly of peptides: toward the design of supramolecular polymers with enhanced chemical and biological functions (https://doi.org:), Prog. Polym. Sci. 123 (2021) 101469, https://doi.org/10.1016/j.progpolymsci.2021.101469.
[105] H. Su, W. Zhang, H. Wang, F. Wang, H. Cui, Paclitaxel-promoted supramolecular polymerization of peptide conjugates, J. Am. Chem. Soc. 141 (2019) 11997–12004.
[106] D. Wu, et al., Polymers with controlled assembly and rigidity made with click-functional peptide bundles, Nature 574 (2019) 658–662.
[107] S. Zhang, Fabrication of novel biomaterials through molecular self-assembly (https://doi.org:), Nat. Biotechnol. 21 (2003) 1171–1178, https://doi.org/10.1038/nbt874.
[108] P. Chakraborty, et al., Nanoengineered peptide-based antimicrobial conductive supramolecular biomaterial for cardiac tissue engineering (https://doi.org:), Adv. Mater. 33 (2021) 2008715, https://doi.org/10.1002/adma.202008715.
[109] F. Gelain, Z. Luo, S. Zhang, Self-assembling peptide EAK16 and RADA16 nanofiber scaffold hydrogel, Chem. Rev. 120 (2020) 13434–13460.
[110] B.B. Hsu, et al., Clotting mimicry from robust hemostatic bandages based on self-assembling peptides, ACS Nano 9 (2015) 9394–9406.
[111] A.N. Moore, J.D. Hartgerink, Self-assembling multidomain peptide nanofibers for delivery of bioactive molecules and tissue regeneration (https://doi.org:), Acc. Chem. Res. 50 (2017) 714–722, https://doi.org/10.1021/acs.accounts.6b00553.
[112] S. Guan, et al., Self-assembled peptide–poloxamine nanoparticles enable in vitro and in vivo genome restoration for cystic fibrosis (https://doi.org:), Nat. Nanotechnol. 14 (2019) 287–297, https://doi.org/10.1038/s41565-018-0358-x.
[113] C.J. Edwards-Gayle, et al., Selective antibacterial activity and lipid membrane interactions of arginine-rich amphiphilic peptides, ACS Appl. Bio Mater. 3 (2020) 1165–1175.
[114] P. Zhang, et al., Peptide-based nanoprobes for molecular imaging and disease diagnostics, Chem. Soc. Rev. 47 (2018) 3490–3529.
[115] S. Bera, et al., Rigid helical-like assemblies from a self-aggregating tripeptide, Nat. Mater. 18 (2019) 503–509.
[116] R. Xing, C. Yuan, W. Fan, X. Ren, X. Yan, Biomolecular glass with amino acid and peptide nanoarchitectonics, eadd8105, Sci. Adv. 9 (2023). eadd8105.
[117] J.Y. Rho, et al., Dual self-assembly of supramolecular peptide nanotubes to provide stabilisation in water, Nat. Commun. 10 (2019) 4708.
[118] S. Bera, et al., Self-assembly of aromatic amino acid enantiomers into supramolecular materials of high rigidity (https://doi.org:), ACS Nano 14 (2020) 1694–1706, https://doi.org/10.1021/acsnano.9b07307.
[119] J.C. Brendel, et al., Secondary self-assembly of supramolecular nanotubes into tubisomes and their activity on cells, Angew. Chem. Int. Ed. 57 (2018) 16678–16682.
[120] M. Danial, My-Nhi Tran, C. Young, P.G. Perrier, S. Jolliffe, K.A. Janus, cyclic peptide–polymer nanotubes, *Nat. Commun.* 4 (2013) 2780.
[121] J.Y. Rho, et al., Probing the dynamic nature of self-assembling cyclic peptide–polymer nanotubes in solution and in mammalian cells, Adv. Funct. Mater. 28 (2018) 1704569.
[122] O. Berger, et al., Light-emitting self-assembled peptide nucleic acids exhibit both stacking interactions and Watson–Crick base pairing, Nat. Nanotechnol. 10 (2015) 353–360.
[123] H. Shaikh, et al., Hydrogel and organogel formation by hierarchical self-assembly of cyclic peptides nanotubes, Chem. –A Eur. J. 24 (2018) 19066–19074.
[124] Q. Song, J. Yang, J.Y. Rho, S. Perrier, Supramolecular switching of the self-assembly of cyclic peptide–polymer conjugates via host–guest chemistry, Chem. Commun. 55 (2019) 5291–5294.
[125] K. Tao, et al., Quantum confined peptide assemblies with tunable visible to near-infrared spectral range, Nat. Commun. 9 (2018) 3217.
[126] Y. Chen, et al., Self-assembly of cyclic dipeptides: platforms for functional materials, Protein Pept. Lett. 27 (2020) 688–697.
[127] C. Alvarado, K. Kazerounian, On the rotational operators in protein structure simulations, Protein Eng. 16 (2003) 717–720.
[128] K. Kazerounian, From mechanisms and robotics to protein conformation and drug design, J. Mech. Des. 126 (2004) 40–45.
[129] Kazerounian, K., Latif, K., Rodriguez, K. & Alvarado, C. in International Design Engineering Technical Conferences and Computers and Information in Engineering Conference. 645-658.
[130] Subramanian, R. & Kazerounian, K. in International Design Engineering Technical Conferences and Computers and Information in Engineering Conference. 601-613.
[131] P. Tavousi, M. Behandish, H.T. Ilieş, K. Kazerounian, Protofold ii: enhanced model and implementation for kinetostatic protein folding, J. Nanotechnol. Eng. Med. (6 () (2015).
[132] P. Tavousi, K. Kazerounian, H. Ilies, Synthesizing functional mechanisms from a link soup, J. Mech. Des. 138 (2016).
[133] M.T. Chorsi, et al., Kinematic design of functional nanoscale mechanisms from molecular primitives, J. Micro Nano-Manuf. 9 (2021).
[134] X. Kong, A variable-DOF single-loop 7R spatial mechanism with five motion modes, Mech. Mach. Theory 120 (2018) 239–249.
[135] D. Baker, A. Sali, Protein structure prediction and structural genomics, Science 294 (2001) 93–96.
[136] Rohl, C.A., Strauss, C.E., Misura, K.M. & Baker, D. in *Methods in enzymology* Vol. 383 66-93 (Elsevier, 2004).
[137] V.K. Mulligan, et al., Computationally designed peptide macrocycle inhibitors of New Delhi metallo-β-lactamase 1, Proc. Natl. Acad. Sci. 118 (2021) e2012800118.
[138] P. Hosseinzadeh, et al., Anchor extension: a structure-guided approach to design cyclic peptides targeting enzyme active sites, Nat. Commun. 12 (1) (2021) 12.
[139] V.K. Mulligan, et al., Computational design of mixed chirality peptide macrocycles with internal symmetry, Protein Sci. 29 (2020) 2433–2445.
[140] M. Amaral, et al., Protein conformational flexibility modulates kinetics and thermodynamics of drug binding, Nat. Commun. 8 (1) (2017) 14.
[141] S. Li, et al., Particle robotics based on statistical mechanics of loosely coupled components, Nature 567 (2019) 361–365.
[142] C. Yuan, et al., Hierarchically oriented organization in supramolecular peptide crystals (https://doi.org:), Nat. Rev. Chem. 3 (2019) 567–588, https://doi.org/10.1038/s41570-019-0129-8.
[143] C. Yuan, et al., Nucleation and growth of amino acid and peptide supramolecular polymers through liquid–liquid phase separation (https://doi.org:), Angew. Chem. Int. Ed. 58 (2019) 18116–18123, https://doi.org/10.1002/anie.201911782.
[144] N.J. Greenfield, Using circular dichroism spectra to estimate protein secondary structure, Nat. Protoc. 1 (2006) 2876–2890.
[145] A.C. Gibbs, et al., Unusual β-sheet periodicity in small cyclic peptides, Nat. Struct. Biol. 5 (1998) 284–288.
[146] R.J. Woods, et al., Cyclic modular β-sheets, J. Am. Chem. Soc. 129 (2007) 2548–2558.
[147] J. Zheng, et al., Macrocyclic β-sheet peptides that inhibit the aggregation of a tau-protein-derived hexapeptide, J. Am. Chem. Soc. 133 (2011) 3144–3157.
[148] R. Chapman, M. Danial, M.L. Koh, K.A. Jolliffe, S. Perrier, Design and properties of functional nanotubes from the self-assembly of cyclic peptide templates, Chem. Soc. Rev. 41 (2012) 6023–6041.
[149] M. Calvelo, et al., Parallel versus antiparallel β-sheet structure in cyclic peptide hybrids containing γ-or δ-cyclic amino acids, Chem. –A Eur. J. 26 (2020) 5846–5858.
[150] A. Ghorai, B. Achari, P. Chattopadhyay, Self-assembly of cyclic peptides and peptidomimetic macrocycles: linking structure with function (https://doi.org:), Tetrahedron 72 (2016) 3379–3387, https://doi.org/10.1016/j.tet.2016.04.071.
[151] D.H.T. Le, et al., Self-Assembly of Elastin–Mimetic Double Hydrophobic Polypeptides (https://doi.org:), Biomacromolecules 14 (2013) 1028–1034, https://doi.org/10.1021/bm301887m.
[152] D. Mandal, A. Nasrolahi Shirazi, K. Parang, Self-assembly of peptides to nanostructures (https://doi.org:), Org. Biomol. Chem. 12 (2014) 3544–3561, https://doi.org/10.1039/c4ob00447g.
[153] C. Wiedemann, A. Kumar, A. Lang, O. Ohlenschläger, Cysteines and disulfide bonds as structure-forming units: insights from different domains of life and the

potential for characterization by NMR (https://doi.org:), Front Chem. 8 (2020) 280, https://doi.org/10.3389/fchem.2020.00280.
[154] S. Rauscher, R. Pomès, Structural disorder and protein elasticity, Fuzziness (2012) 159–183.
[155] G. Wei, et al., Self-assembling peptide and protein amyloids: from structure to tailored function in nanotechnology, Chem. Soc. Rev. 46 (2017) 4661–4708.
[156] C. Diaferia, et al., The introduction of a cysteine residue modulates the mechanical properties of aromatic-based solid aggregates and self-supporting hydrogels, Chem. –A Eur. J. 27 (2021) 14886–14898.
[157] C. Yuan, Q. Li, R. Xing, J. Li, X. Yan, Peptide self-assembly through liquid-liquid phase separation (https://doi.org:), Chem 9 (2023) 2425–2445, https://doi.org/10.1016/j.chempr.2023.05.009.
[158] L.R. Volpatti, T.P. Knowles, Polymer physics inspired approaches for the study of the mechanical properties of amyloid fibrils, J. Polym. Sci. Part B: Polym. Phys. 52 (2014) 281–292.
[159] P.A. Guerette, D.G. Ginzinger, B.H. Weber, J.M. Gosline, Silk properties determined by gland-specific expression of a spider fibroin gene family, Science 272 (1996) 112–115.
[160] L. Yang, et al., Micromechanical bending of single collagen fibrils using atomic force microscopy, J. Biomed. Mater. Res. Part A 82 (2007) 160–168.
[161] N. Sasaki, S. Odajima, Elongation mechanism of collagen fibrils and force-strain relations of tendon at each level of structural hierarchy, J. Biomech. 29 (1996) 1131–1136.
[162] R. Bonser, P. Purslow, The Young's modulus of feather keratin, J. Exp. Biol. 198 (1995) 1029–1033.
[163] A.M. Peattie, C. Majidi, A. Corder, R.J. Full, Ancestrally high elastic modulus of gecko setal β-keratin, J. R. Soc. Interface 4 (2007) 1071–1076.
[164] P. Hosseinzadeh, et al., Comprehensive computational design of ordered peptide macrocycles, Science 358 (2017) 1461–1466.
[165] G. Bhardwaj, et al., Accurate de novo design of hyperstable constrained peptides, Nature 538 (2016) 329–335.
[166] P. Tavousi, M. Behandish, H.T. Ilieş, K. Kazerounian, Protofold ii: Enhanced model and implementation for kinetostatic protein folding, J. Nanotechnol. Eng. Med. 6 (2015) 034601.
[167] R.F. Alford, et al., The Rosetta all-atom energy function for macromolecular modeling and design, J. Chem. Theory Comput. 13 (2017) 3031–3048.
[168] J.C. Phillips, et al., Scalable molecular dynamics with NAMD, J. Comput. Chem. 26 (2005) 1781–1802.
[169] K. Vanommeslaeghe, et al., CHARMM general force field: a force field for drug-like molecules compatible with the CHARMM all-atom additive biological force fields, J. Comput. Chem. 31 (2010) 671–690.
[170] D.J. Burgess, B.D. Huey, C. Srinivasan, M. Zhao, Rate- and depth-dependent nanomechanical behavior of individual living Chinese hamster ovary cells probed by atomic force microscopy (https://doi.org:), J. Mater. Res. 21 (2006) 1906–1912, https://doi.org/10.1557/jmr.2006.0233.